Glycolysis-related lncRNA may be associated with prognosis and immune activity in grade II-III glioma

TAO YANG[1,2*], RUIGUANG ZHANG[1*], ZHENFEN CUI[2*], BOWEN ZHENG[1], XIAOWEI ZHU[1], XINYU YANG[1] and QIANG HUANG[1]

[1]Department of Neurosurgery, Tianjin Medical University General Hospital, Tianjin 300000; [2]Department of Neurosurgery, Heji Hospital Affiliated to Changzhi Medical College, Changzhi, Shanxi 046000, P.R. China

Received November 19, 2023; Accepted March 4, 2024

DOI: 10.3892/ol.2024.14371

Abstract. Glucose metabolism, as a novel theory to explain tumor cell behavior, has been intensively studied in various tumors. The present study explored the long non-coding RNAs (lncRNAs) related to glycolysis in grade II-III glioma, aiming to provide a promising target for further research. Pearson correlation analysis was used to identify glycolysis-related lncRNAs. Univariate/multivariate Cox regression analysis and the Least Absolute Shrinkage and Selection Operator algorithm were applied to identify glycolysis-related lncRNAs to construct a prognosis prediction model. Subsequently, multi-dimensional evaluations were used to verify whether the risk model could predict the prognosis and survival rate of patients with grade II-III glioma. Finally, it was verified by functional experiments. The present study finally identified seven glycolysis-related lncRNAs (CRNDE, AC022034.1, RHOQ-AS1, AL159169.2, AL133215.2, AC007098.1 and LINC02587) to construct a prognosis prediction model. The present study further investigated the underlying immune microenvironment, somatic landscape and functional enrichment pathways. Additionally, individualized immunotherapeutic strategies and candidate compounds were identified to guide clinical treatment. The experimental results demonstrated that CRNDE could increase the proliferation of SHG-44 cells. In conclusion, a large sample of human grade II-III glioma in The Cancer Genome Atlas database was used to construct a risk model using glycolysis-related lncRNAs to predict the prognosis of patients with grade II-III glioma.

Correspondence to: Professor Qiang Huang, Department of Neurosurgery, Tianjin Medical University General Hospital, 154 Anshan Road, Heping, Tianjin 300000, P.R. China
E-mail: 13734230629@163.com

*Contributed equally

Key words: low-grade glioma, long non-coding RNA, glucose metabolism, immune microenvironment, glycolysis

Introduction

Gliomas are the most common malignant tumors of the central nervous system (CNS) (1). The World Health Organization classifies glioma as grade I-IV (2,3). Although the study of grade II-III glioma has improved clinical treatment, numerous patients with grade II-III glioma will relapse later, resulting in poor prognosis and reduced quality of life (4). As a result of this prognostic heterogeneity, the molecular classification should be incorporated into the evaluation of patients with grade II-III glioma. As precision medicine becomes increasingly prevalent, traditional markers such as mutations of the isocitrate dehydrogenase gene and deletions of chromosome 1p and 19q may not be sufficient for individual risk assessment of patients with grade II-III glioma (5,6). Therefore, it is imperative that novel biomarkers are identified that are effective in optimizing their treatment.

Changes in energy metabolism are one of the most significant biological characteristics associated with cancer (7). The Warburg effect refers to the change from oxidative phosphorylation to aerobic glycolysis, which can provide energy for cancer cells (8).

The metabolism of cancer cells is reprogrammed to improve glucose uptake, so it can also provide more energy to cancer cells, even though aerobic glycolysis produces less energy than mitochondrial oxidative phosphorylation (9,10). There is increasing evidence that this reprogramming of metabolic activity by tumor cells serves an important role in the development of various cancer types (11,12). The glycolysis-related risk model constructed by Liu *et al* (13) provided an improved understanding of rectal cancer. Additionally, Reuss *et al* (14) found that ketogenic diets for management targeting the Warburg effect could effectively halt the progression of grade II-III glioma to more aggressive subtypes. Long non-coding RNAs (lncRNAs) are a class of RNA molecules with specific functions that participate in genome organization, cell structure and gene expression through a variety of interactions. lncRNAs regulate gene expression through epigenetic regulation, transcriptional regulation and post-transcriptional regulation, thereby participating in biological processes such as cell proliferation, differentiation and apoptosis in cancer (15). In recent years, lncRNAs have been found to be involved in tumor cell growth, proliferation and energy

acquisition (16,17). For example, LINC00092 directly binds to 6-phosphofructo-2-kinase/fructose-2,6-biphosphatase 2 to promote tumorigenesis (18). Sun *et al* (19) constructed a prognostic risk model to predict Lung adenocarcinoma patient's survival and response to immunotherapy based on hub oxidative stress-related lncRNAs using bioinformatics analysis. As a result of these newly identified features, prognosis can be more accurately predicted and a greater understanding of how lncRNAs contribute to cancer development can be gained.

The present study demonstrated a potential association between glycolysis-related lncRNAs and grade II-III glioma using bioinformatics approaches. The present results may be helpful to understand the cell energy metabolism of grade II-III glioma in the future.

Materials and methods

Data acquisition. All the information of patients with grade II-III glioma was obtained from The Cancer Genome Atlas database (Center for Cancer Genomics at the National Cancer Institute; https://portal.gdc.cancer.gov/). The Perl language (http://www.perl.org/) was used to merge RNA-sequencing results into matrix files. The data of 479 patients were obtained and the patients were randomly divided into two groups using the R (version 4.2.3; http://www.R-project.org/) package 'caret' (20). The first group (n=240) was used for training and the other group (n=239) was used for testing. All data regarding the clinical characteristics of all patients are shown in Table SI.

Glycolysis-related gene acquisition. A total of 243 glycolysis-related gene profiles (21) (Table SII) were obtained from the Molecular Signatures Database (http://www.gsea-msigdb.org) labeled 'Hallmark glycolysis' and 'Kyoto Encyclopedia of Genes and Genomes (KEGG) glycolysis gluconeogenesis'.

Screening glycolysis-related lncRNAs. The lncRNA annotation files were obtained from the Generic Code Database (https://www.gencodegenes.org/human/). Subsequently, lncRNA information related to glycolysis-related gene expression was obtained. The selection criteria were set as $|R|>0.5$ and $P<0.001$.

Construction of seven glycolysis-related lncRNAs prognostic signature and risk model. The training set was used to construct the prognostic model. As previously reported by Sun *et al* (22), a gene signature with high performance and stability was constructed using a combination of machine learning algorithms, including the Least Absolute Shrinkage and Selection Operator (LASSO) algorithm, and multivariate Cox analyses. Univariate Cox analysis was applied to determine which glycolysis-related lncRNAs were associated with overall survival (OS) among patients with grade II-III glioma ($P<0.05$). Subsequently, LASSO regression analysis was conducted to analyze the glycolysis-related lncRNAs using the package 'glmnet' in R (23). Upon reaching the minimum partial likelihood deviance, the optimal lambda was identified. Finally, a risk characteristics and prognosis model based on seven glycolysis-related lncRNAs was constructed as follows:

$$Risk\ score = \sum_{k=1}^{n} Coef(lncRNA) * expr(lncRNA^{k})$$

Coef (lncRNA) refers to the coefficient associated with survival. Expr is the expression of lncRNAs.

Validation of the seven glycolysis-related lncRNAs risk model. Kaplan-Meier (K-M) analysis was applied to compare OS between two groups using the R package 'survival' (24) (version 3.5-0). The package 'timeROC'(25) (version 0.4) was used to verify the predictive ability of the established risk model. The concordance index (C-index) was estimated to evaluate the discrimination of the model. Principal component analysis (PCA) and t-distributed stochastic neighbor embedding (t-SNE) analysis were used to visually distinguish two groups.

Construction and assessment of the nomogram. Independent prognostic factor analysis was conducted in R with the package 'survival'. The R package 'rms' (26) was further applied to construct a nomogram and the predictive ability of the nomogram was evaluated.

Exploration of the tumor immune microenvironment and tumor mutation burden (TMB). To quantitatively analyze tumor tissue transcriptomic data, the CIBERSORT algorithm was used, which led to the estimation of the absolute number of immune and stromal cells present in the tumor tissues. Furthermore, the single sample Gene Set Enrichment Analysis (ssGSEA) algorithm was used to assess the difference between high- and low-risk groups in terms of the ability to resist tumor infiltration (27). The ESTIMATE algorithm was used to determine the stromal score, immune score and ESTIMATE score of grade II-III glioma samples (28). The package 'maftools' was used to analyze the TMB (29).

Exploration of the therapeutic significance of the risk model. Drug information was obtained from the Genomics of Cancer Drug Sensitivity (GDSC) website (30) (http://www.cancerrxgene.org), and the R package 'pRRophetic' (31) was used to predict IC_{50} values to explore possible clinical adjuvant drugs for the treatment of grade II-III glioma (https://www.cancerrxgene.org). To determine if the risk model was associated with immunotherapy, the expression levels of key genes in the two groups of immune checkpoints were compared.

Functional enrichment analysis. Differentially expressed genes (DEGs) were identified using the package 'limma' (32). The 'clusterProfiler' package was used to study the related functions and pathways of DEGs bias (33). GSEA was used to compare potential pathways between the two groups. The R package 'ggalluvival' (34) (version 0.12.5) was used to visualize the association between lncRNAs and risk factors (protective/risk) in a Sankey diagram.

Construction of the lncRNA-mRNA co-expression network. Cytoscape software (version 3.9.0; http://cytoscape.org) was used to visualize the lncRNA-mRNA co-expression network.

Cell culture. The HA1800 human normal astrocyte cell line and the SHG-44 human glioma cell line were purchased from American Type Culture Collection (35). HA1800 and SHG-44 cells were cultured in DMEM (Gibco; Thermo Fisher Scientific, Inc.) supplemented with 10% fetal bovine serum (Gibco; Thermo Fisher Scientific, Inc.) and antibiotics (100 U/ml penicillin and 100 μg/ml streptomycin). Cells were incubated at 37˚C with 5% CO_2.

Transfection. Colorectal neoplasia differentially expressed (CRNDE) small interfering RNA (siRNA), si-CRNDE-1 (5'-GGTGTTAAGTGTGATGCTTCC-3') or siCRNDE-2 (5'-GGATGCTGTCAGCTAAGTTCA-3'), and negative control siRNA (5'-UUCUCCGAACGUGUCACGUTT-3') were purchased from Shanghai GenePharma Co., Ltd (cat. no. A10001). CRNDE expression in SHG-44 cells was silenced by siRNA transfection using Lipofectamine® RNAiMax reagent (Invitrogen; Thermo Fisher Scientific, Inc.) according to the manufacturer's instructions. The transfection compound was prepared at room temperature for 20 min. The concentration of siRNA used was 50 nM. After culturing in the incubator (37˚C) for 48 h, the cells and cell cultures were harvested for subsequent experiments, and the transfection efficiency was evaluated by reverse transcription-quantitative PCR (RT-qPCR).

RT-qPCR. The cell density for RNA extraction was $1x10^6$. Total RNA was extracted using the TRIzol® reagent (Thermo Fisher Scientific, Inc.), and cDNA was obtained by reverse transcription using the TransScript® First-Strand cDNA Synthesis SuperMix (Shanghai Yeasen Biotechnology Co., Ltd.). The cDNA was amplified using the Hieff UNICON universal Blue qPCR SYBR Green Master Mix kit (YEASEN Corporation, China). RNA extraction, cDNA synthesis and qPCR were all performed according to the manufacturer's protocols. The reaction volume was 20 μl, including 10 μl of Universal Blue qPCR SYBR Green Master Mix, 7.6 μl of nucleic acid-free water, 0.2 μl of each primer, and 2 μl of cDNA product. The PCR cycling conditions were as follows: 95˚C for 2 min for 1 cycle, 95˚C for 10 sec and 60˚C for 30 sec for 40 cycles, and the melting curve was then determined. GAPDH was used as an internal reference and relative mRNA expression was calculated using the $2^{-\Delta\Delta Cq}$ method (36,37). The experiment was repeated three times. The primer sequences were as follows: GAPDH forward, 5'-AAGGTGAAGGTCGGAGTCAAC-3' and reverse, 5'-GGGGTCATTGATGGCAACAAT-3'; and CRNDE forward, 5'-TGGATGCTGTCAGCTAAGTTCAC-3' and reverse, 5'-TTCCAGTGGCATCCTCCTTATC-3'.

Cell Counting Kit-8 (CCK-8) assays. The effect of CRNDE expression on the proliferation of SHG-44 cells was detected using a CCK-8 assay (Dojindo Laboratories, Inc.). Briefly, after the cells were cultured in 96-well plates ($6x10^3$ cells/well) for 0, 24, 48, 72 and 96 h, 20 μl CCK-8 cell proliferation agent was added to each well and incubated for 2 h at 37˚C and the absorbance of the cell culture medium was measured at a wavelength of 450 nm.

Colony formation assays. After transfection, SHG-44 cells were cultured in 6-well plates ($5x10^3$ cells/well) for 12 days. After fixation with 4% paraformaldehyde solution at room temperature for 20 min, the cells were stained with 0.1% crystal violet at room temperature for 15 min (Beyotime Institute of Biotechnology).

Measurement of the extracellular acidification rate (ECAR). SHG-44 cells were seeded in 6-well plates ($3x10^5$ cells/well) and incubated for 24 h. Prior to the assay, cells were subjected to serum deprivation to enhance glucose uptake. Subsequently, the cells were washed three times with PBS buffer. Following this, the cells were stimulated with 100 nM insulin for 30 min. A glucose uptake assay kit (Abcam) was used to quantify glucose uptake, with all results being normalized to the cell number.

Statistical analysis. All statistical analyses were conducted in the R and Perl software and the statistical results of samples were expressed as mean ± standard deviation. All assays were done at least three times independently. Independent Student's t-tests were applied to determine the difference between the two groups. Correlation analysis was performed using the Pearson correlation test. For the analysis of differences between K-M curves, the log-rank test was performed. If there is no special description for the above method, $P<0.05$ was considered to indicate a statistically significant difference.

Results

Screening of glycolytic lncRNAs in patients with low-grade glioma. Fig. 1 shows the process of the present study. A total of 14,056 lncRNAs and 243 glycolytic genes were screened for subsequent Pearson correlation analysis (21). The co-results among lncRNAs and mRNAs of Pearson correlation test are shown in Table SIII and 1,889 glycolytic lncRNAs were identified. Additionally, the consistent part of the expression between glycolytic genes and glycolytic lncRNAs was shown in the Sankey diagram, and their correlation was visually demonstrated (Fig. 2A and B).

Constructing a glycolytic lncRNAs risk model. Univariate Cox analysis was used to screen glycolytic lncRNAs. In the end, 656 prognostic lncRNAs were identified in the training set (Table SIV). LASSO regression analysis was performed on these survival-related lncRNAs to further screen key lncRNAs for model construction. Finally, nine lncRNAs were retained (Fig. 2C and D). Subsequently, multivariate Cox regression analysis was performed and seven glycolytic lncRNAs, including CRNDE, AC022034.1, Ras homolog family member Q (RHOQ-AS1), AL159169.2, AL133215.2, AC007098.1 and LINC02587, were identified (Fig. 2E; Table SV). Finally, the calculation formula was determined using the Cox regression model coefficient and lncRNA expression: CRNDE x 0.530754428201569 + AC022034.1 x 0.51597198629815 + RHOQ-AS1 x 4.0070016692408 + AL159169.2 x-1.33589967405211 + AL133215.2 x 0.902923079138878 + AC007098.1 x 0.660037199843563 + LINC02587 x 0.29755586476417. AL159169.2, with a negative coefficient, tended to be a protective factor, and the other six lncRNAs tended to be risk factors, which was confirmed by the Sankey diagram (Fig. 3A). Additionally, the relative

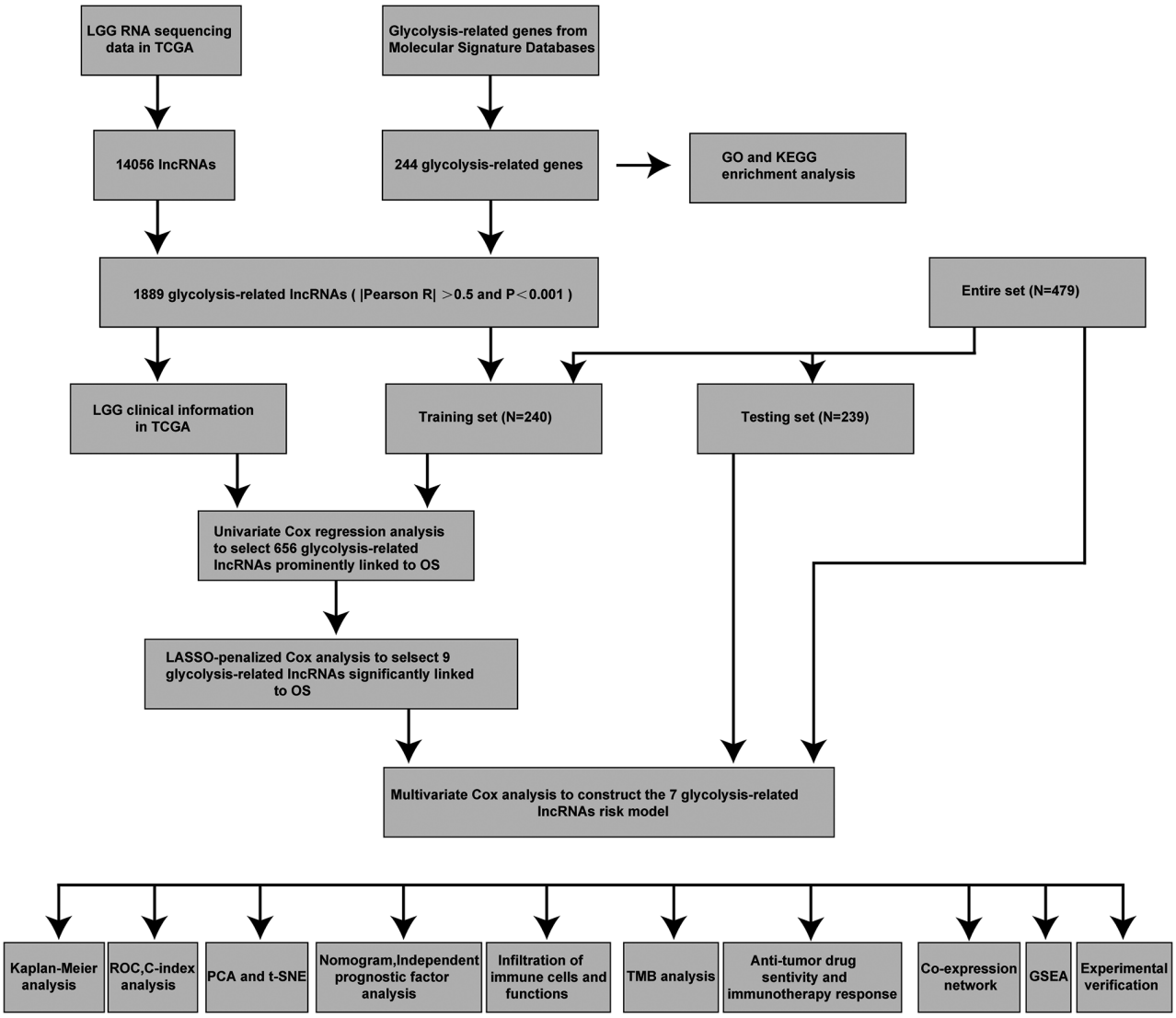

Figure 1. Workflow of the present study. C-index, concordance index; GO, Gene Ontology; GSEA, Gene Set Enrichment Analysis; KEGG, Kyoto Encyclopedia of Genes and Genomes; LASSO, Least Absolute Shrinkage and Selection Operator; LGG, low-grade glioma; lncRNA, long non-coding RNA; OS, overall survival; PCA, principal component analysis; ROC, receiver operating characteristic; t-SNE, t-distributed stochastic neighbor embedding; TCGA, The Cancer Genome Atlas; TMB, tumor mutation burden.

expression levels of the seven hub glycolytic lncRNAs were evaluated (Fig. 3B). Patients in the high-risk group had higher expression levels of destructive lncRNAs than patients in the low-risk group (Fig. 3A and B). Subsequently, the performance of the risk formula was verified using PCA and t-SNE algorithms. The results indicated that there was a difference between the two groups of patients with grade II-III glioma, which clearly showed that the situation of patients with grade II-III glioma in the two groups was different (Fig. 3C and D). Furthermore, the survival of the two groups of patients with grade II-III glioma in the training set were compared (Fig. 3E). The OS of different groups in the training set was compared by K-M analysis. The results demonstrated that patients with grade II-III glioma in the low-risk group had an improved OS (Fig. 3F; P<0.001). The receiver operating characteristic curve showed that the seven glycolytic lncRNAs had high accuracy in diagnostic efficacy, and the areas under the curve (AUCs) of 1-, 3- and 5-year prediction were 0.931, 0.921 and 0.866, respectively (Fig. 3G). The C-index of the risk model also showed that the risk model had good reliability (Fig. 3H).

Confirmation of glycolytic lncRNAs risk model. The test set of patients with grade II-III glioma was subsequently used to evaluate the reliability of the model (n=239). K-M analysis indicated the survival of the two groups of patients with grade II-III glioma, and the results demonstrated that the OS of the low-risk group was improved compared with that of the high-risk group (Fig. 4A; P<0.001). Fig. 4B-D shows the distribution of the risk scores, survival time in the two groups and the expression of the seven lncRNAs in the test set. There was a notable difference between the two groups in the PCA and t-SNE analysis (Fig. 4E and F). In the test set, the predicted AUC values of the risk model for 1, 3 and 5 years were 0.846, 0.833 and 0.788, respectively (Fig. 4G). C-index analysis also illustrated that the risk model had good reliability (Fig. 4H). Finally, the entire set of patients with grade II-III glioma (n=479) was used to verify the prognostic ability of the model,

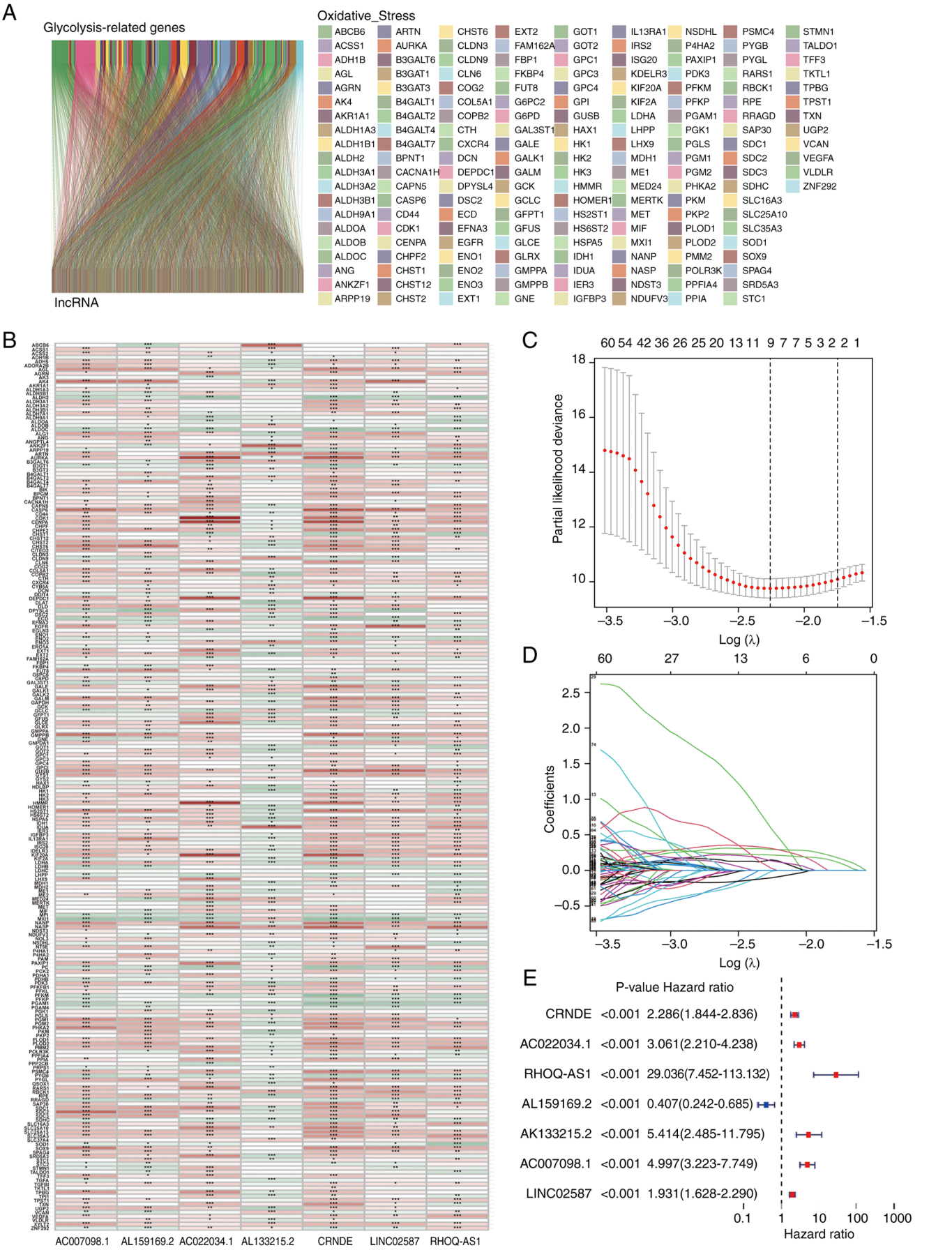

Figure 2. Identification of glycolysis-related lncRNAs and model construction. (A) Sankey relation diagram for glycolysis-related genes and glycolysis-related lncRNAs. (B) Heatmap of the correlation between glycolysis genes and hub glycolysis-related lncRNAs. (C and D) Least Absolute Shrinkage and Selection Operator regression analysis identified nine glycolysis-related lncRNAs. (E) Multivariate Cox regression analysis identified seven glycolysis-related lncRNAs. (*P<0.05; **P<0.01; ***P<0.001). lncRNA, long non-coding RNA.

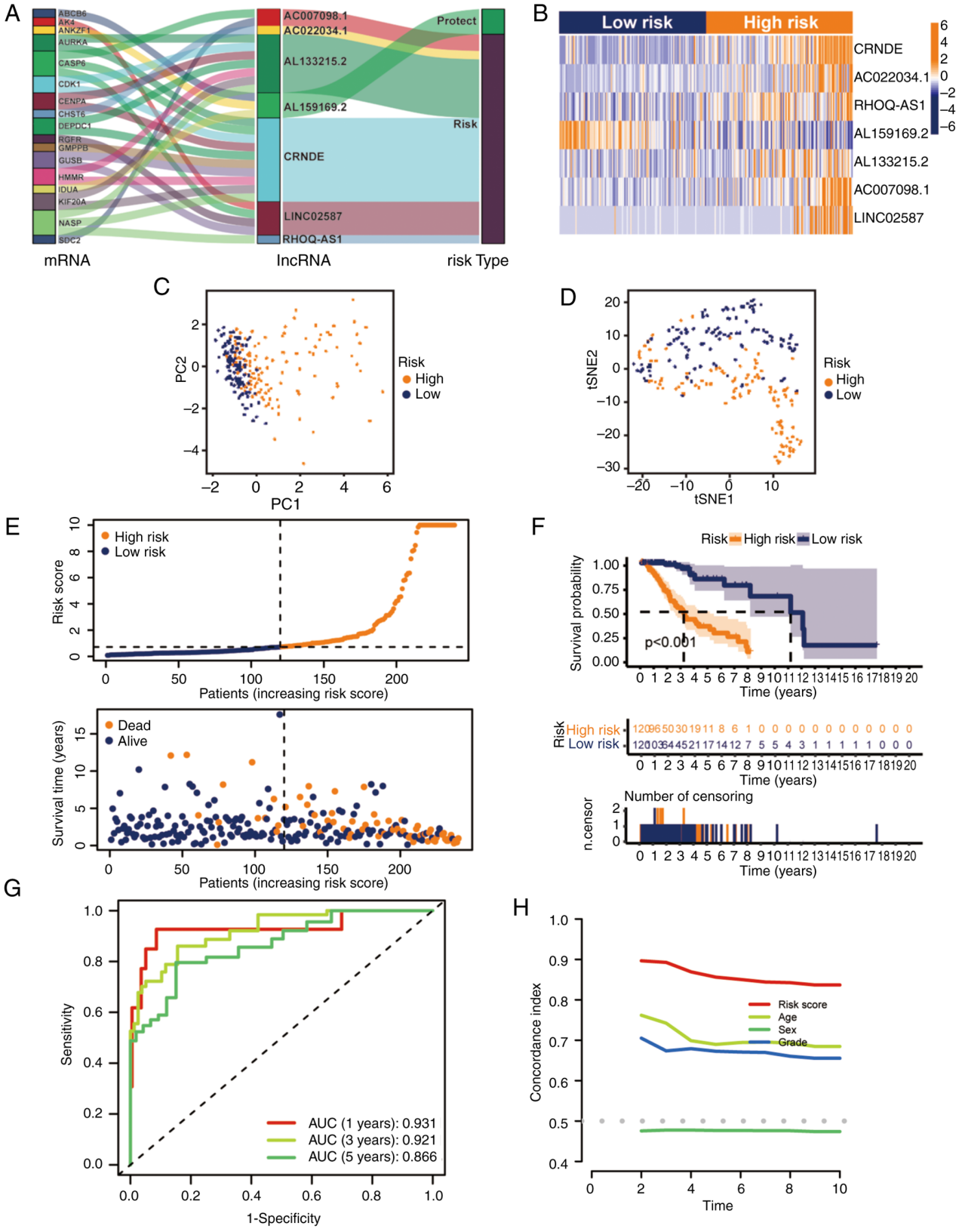

Figure 3. Prognostic value of the risk model of the seven glycolysis-related lncRNAs in the training set. (A) Sankey diagram showing the connection degree among glycolysis mRNAs, glycolysis-related lncRNAs and risk types. (B) relative expression levels of seven hub lncRNAs. (C) PC analysis results and (D) t-SNE results. (E) distribution of risk scores, survival status and survival time patterns. (F) Kaplan-Meier analysis results. (G) receiver operating characteristic curves for 1-, 3- and 5-year overall survival using the risk model, and (H) concordance index analysis based on the training set. AUC, area under the curve; lncRNA, long non-coding RNA; PC, principal component; tSNE, t-distributed stochastic neighbor embedding.

indicating consistency with the aforementioned validation (Fig. 4I-P). It was evident that the established risk model was capable of reliably distinguishing patients with grade II-III glioma based on their risk profile.

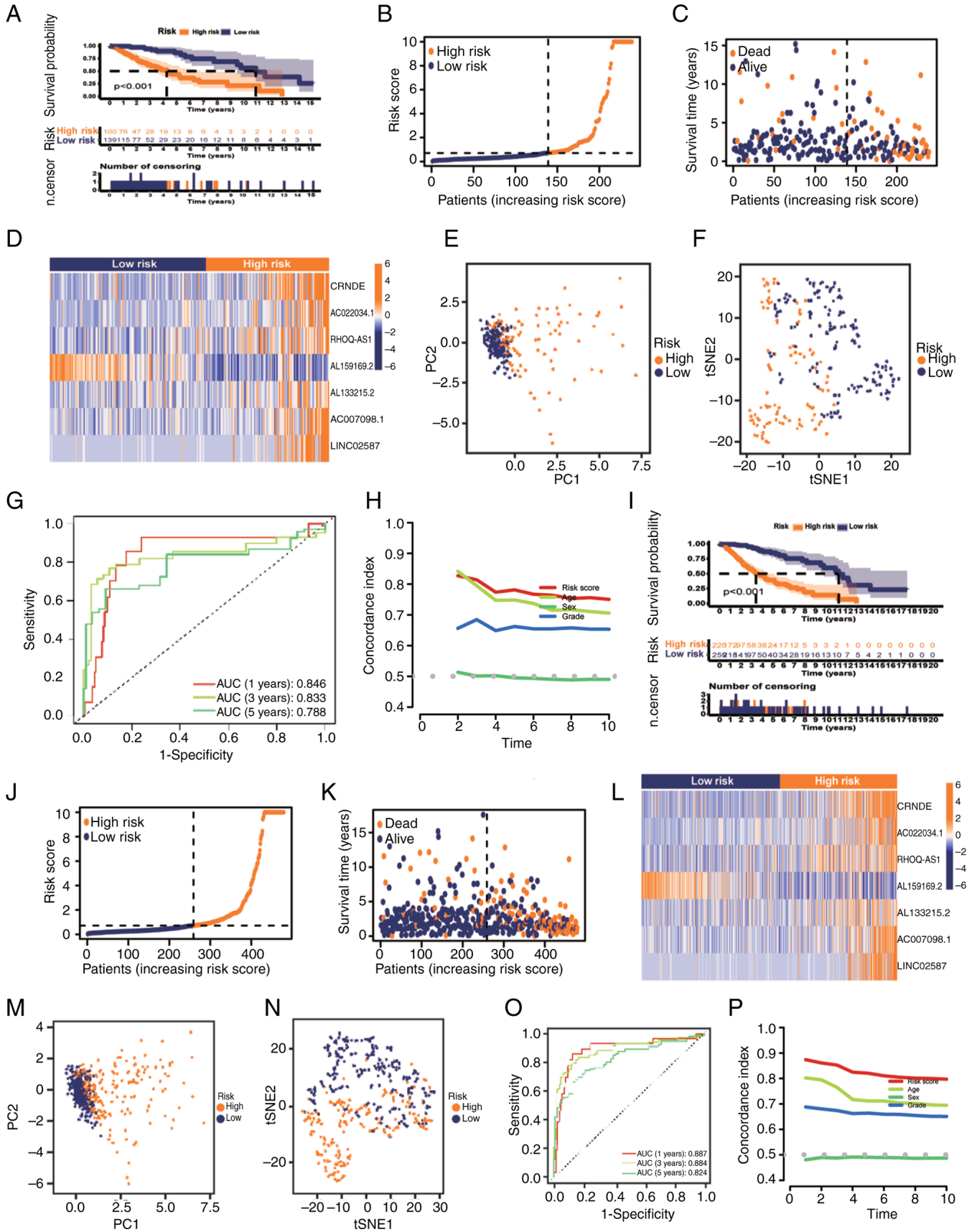

Figure 4. Prognostic value of the risk model of the seven glycolysis-related lncRNAs in the testing and entire sets. (A) K-M analysis results, (B) distribution of risk scores, (C) survival status and survival time patterns, (D) relative expression levels of seven hub lncRNAs, (E) PCA results, (F) tSNE results, (G) ROC curves for 1-, 3- and 5-year OS using the risk model, and (H) C-index analysis based on the testing set. (I) K-M analysis results, (J) distribution of risk scores, (K) survival status and survival time patterns, (L) relative expression levels of seven hub lncRNAs, (M) PCA results, (N) tSNE results, (O) ROC curves for 1-, 3- and 5-year OS using the risk model and (P) Concordance index analysis based on the entire set. AUC, area under the curve; K-M, Kaplan-Meier; lncRNA, long non-coding RNA; OS, overall survival; PC, principal component; PCA, principal component analysis; ROC, receiver operating characteristic; tSNE, t-distributed stochastic neighbor embedding.

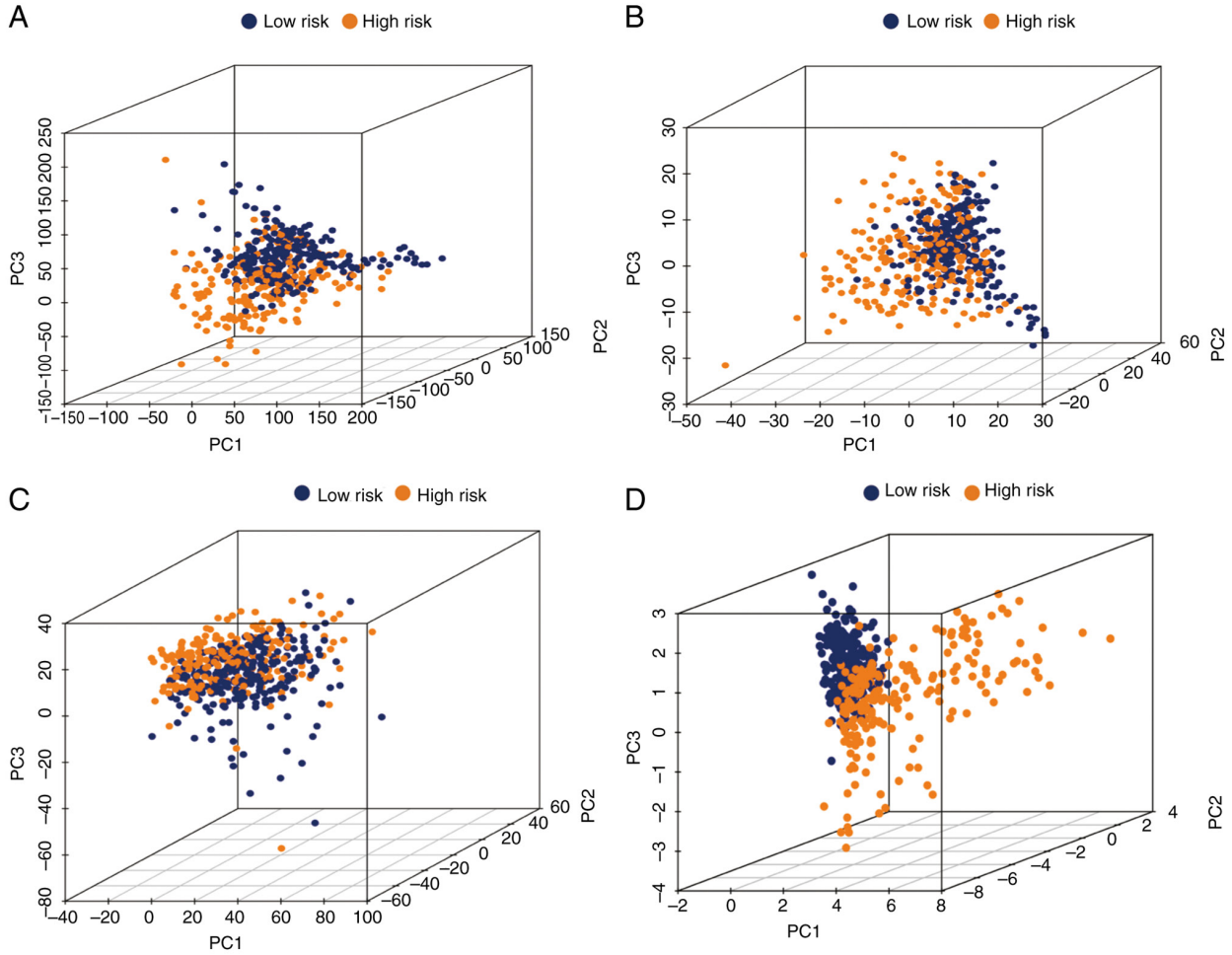

Figure 5. PC analysis of the distributions of the low- and high-risk groups based on (A) the entire gene expression profiles, (B) 243 glycolysis-related gene profiles, (C) 1,889 glycolysis-related long non-coding RNAs and (D) the risk model. PC, principal component.

PCA. To further estimate the distribution of the two groups, PCA was conducted using the whole gene expression profile, 243 glycolytic gene profiles, 1,889 glycolysis-related lncRNAs and the risk model (Fig. 5A-D). This risk model clearly indicated that patients with grade II-III glioma could be correctly classified by the metabolism of glycolysis between the two groups.

Independence of prognostic signature and construction of the nomogram. The next step was to verify the accuracy of the model based on seven lncRNAs associated with glycolysis for independent prediction of prognosis in grade II-III glioma. This was performed using univariate and multivariate Cox regression analysis. The results of univariate regression analysis [hazard ratio (HR), 1.003; 95% CI, 1.002-1.004; P<0.001] indicated that the model could accurately predict the prognosis of patients, and multivariate regression analysis (HR, 1.002; 95% CI, 1.001-1.003; P<0.001) also revealed similar results (Fig. 6A and B). In summary, the risk model was an independent prognostic factor for grade II-III glioma. A nomogram was constructed by combining multiple clinical factors with the constructed risk score to predict the survival rates of patients with grade II-III glioma (38) (Fig. 6C). Subsequently, the reliability of the nomogram was verified, and the results demonstrated that the actual observed value was similar to the predicted value (Fig. 6D). Additionally, the AUC values for the OS rate at each time point were 0.887, 0.884 and 0.825, respectively (Fig. 6E). Compared with the C-index of other clinical features, the nomogram and risk score had higher values (Fig. 6F).

Evaluation of the tumor microenvironment (TME). In view of the extensive research on the TME in the evaluation and treatment of grade II-III glioma, a number of immune assessment methods were applied to determine the difference in the degree of immune infiltration between the two subgroups. First, some basic scores of patients with grade II-III glioma were analyzed using the ESTIMATE algorithm. The results of this indicated that with the increase of the risk level of patients with grade II-III glioma, the immune, stromal and ESTIMATE scores also increased (Fig. 7A-C). Using gene set variation analysis, it was revealed that high-risk grade II-III glioma was related to the change of some immune functions such as 'cytolytic_activity', 'inflammation-promoting' and 'CCR' (Fig. 7D). Subsequently, the categories and proportions of immune cells were analyzed using the CIBERSORT algorithm. The distribution differences and proportion changes of immune cells in the two groups were analyzed (Fig. 7E and F). Additionally, which immune cells were more common in high-risk populations was summarized (Fig. 7G.

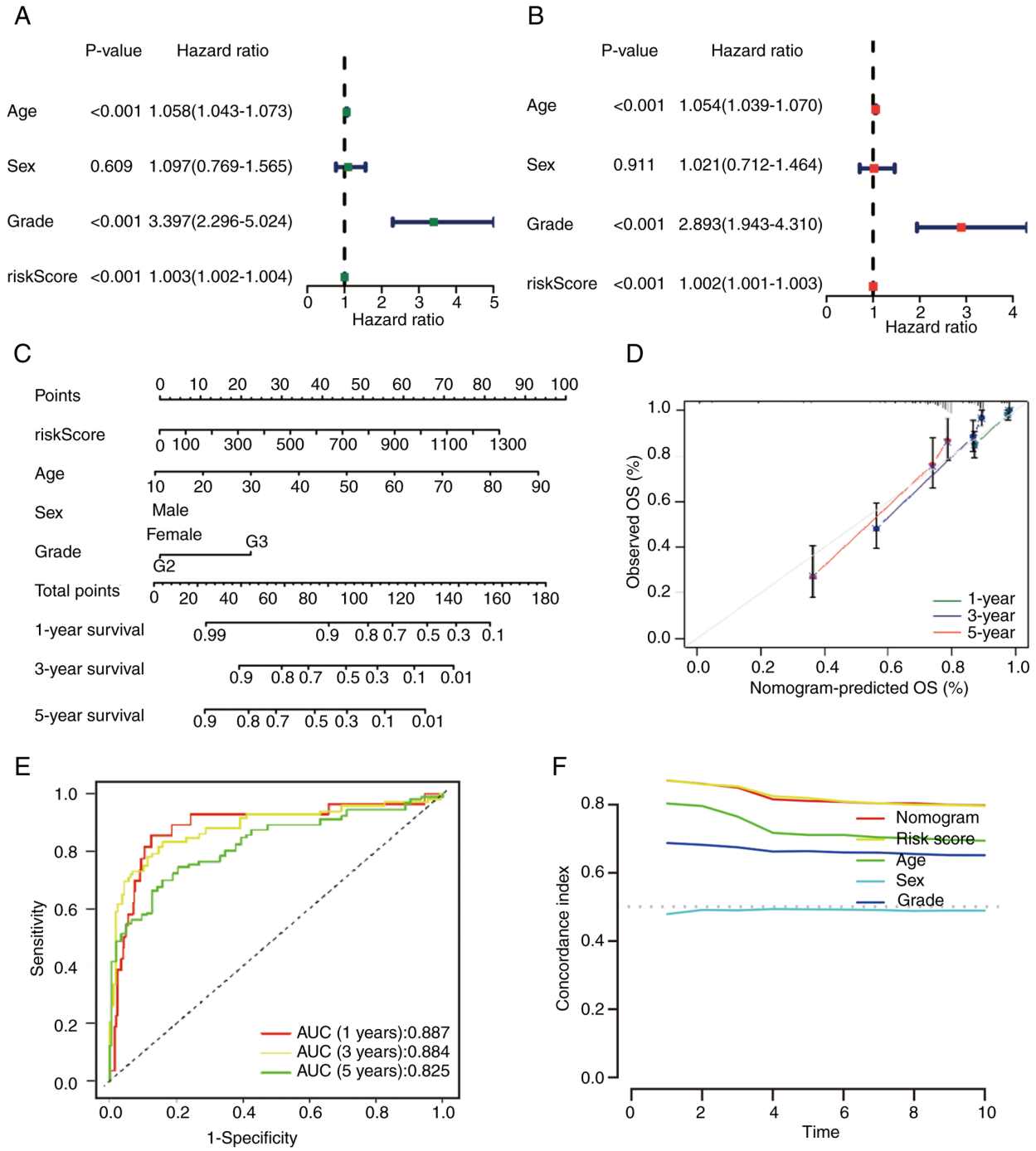

Figure 6. Independence of the prognostic signature and construction of a nomogram. (A) Univariate and (B) multivariate analysis of the association of clinical characteristics and the risk score with OS. (C) Nomogram and (D) calibration curves of the nomogram predicting the probability of OS. (E) Receiver operating characteristic curves of the nomogram predicting the probability of 1-, 3- and 5-year OS. (F) Concordance index analysis of the nomogram. AUC, area under the curve; OS, overall survival.

Finally, the immune cell infiltration of patients with grade II-III glioma in different risk groups was studied using the ssGSEA algorithm. The results indicated that the number of immune cell subsets in the high-risk group was higher (Fig. 7H). Additionally, some important immune functions were significantly upregulated in the high-risk group (Fig. 7I). In summary, it could be seen that patients with grade II-III glioma in the high- and low-risk groups had distinct immune infiltration differences, which may lead to differences in prognosis between the two groups.

Analysis of somatic mutation landscape. TMB is a molecular marker that is used to quantify the mutations that tumor cells take as part of immunotherapy. It can evaluate whether immunotherapy is effective. The present study further explored the somatic mutation rate in the high- and low-risk groups. The results demonstrated that the mutation rate of the low-risk group [241 cases (97.57%) in 247 samples] appeared to be higher than that of the high-risk group [185 cases (85.65%) in 216 samples]. The top-ranked driver mutant genes are shown in Fig. 8A and B. Further quantitative analysis demonstrated

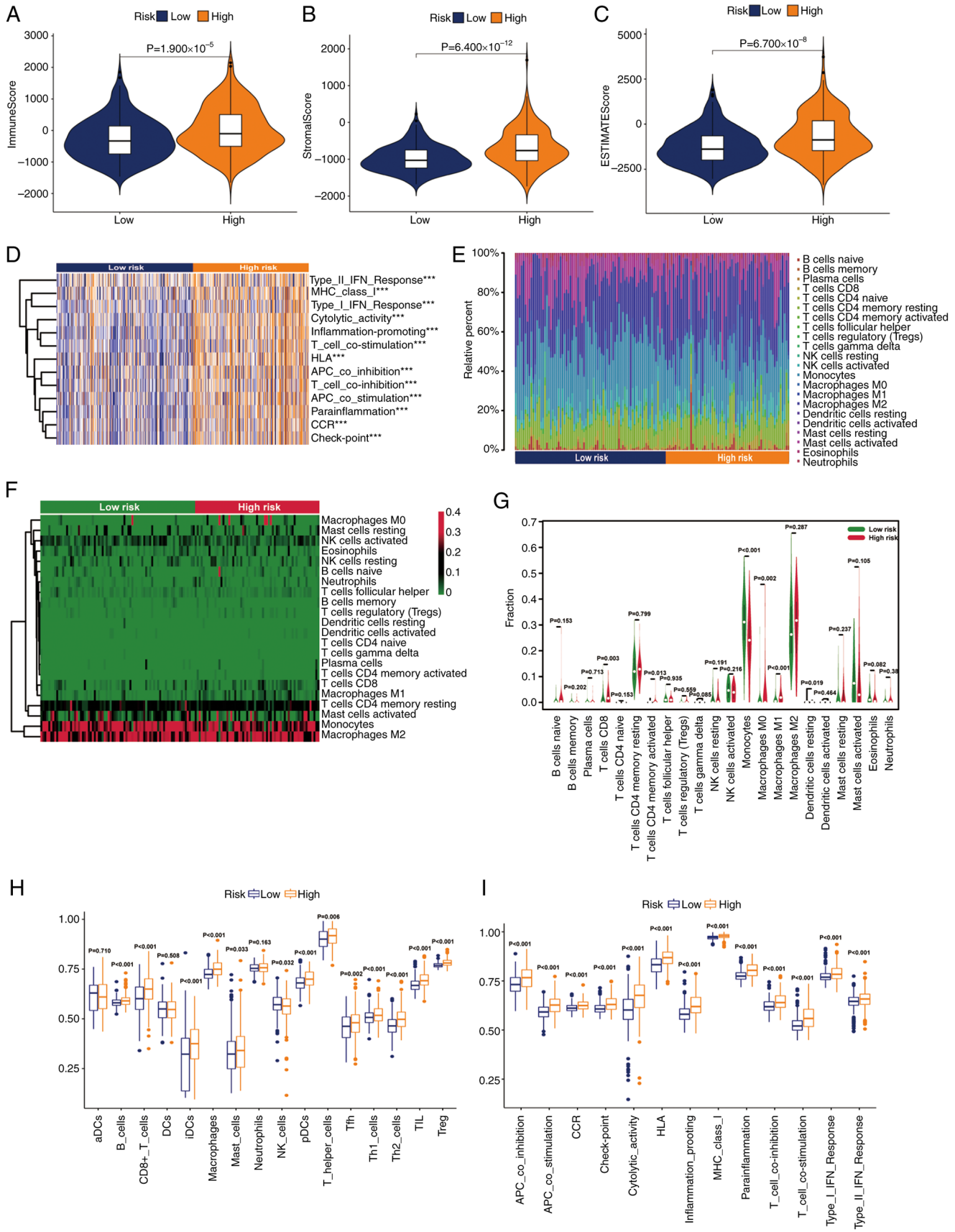

Figure 7. Stratification analysis of the risk score in immune features. Differences in the (A) immune score, (B) stromal score and (C) ESTIMATE score. (D) Gene set variation analysis of immune-related pathways in the two groups. (Expression features of 22 immune cells in a (E) box plot, (F) heatmap and (G) violin plot based on the CIBERSORT algorithm. Differences in the (H) immune cells and (I) immune functions based on the single sample Gene Set Enrichment Analysis algorithm (***P<0.001). ns, not significant; aDC, activated dendritic cell; APC, adenomatous polyposis coli; CCR, chemokine receptor; DC, dendritic cell; HLA, human leukocyte antigen; iDC, immature dendritic cell; MHC, major histocompatibility complex; NK, natural killer; pDC, plasmacytoid dendritic cell; Tfh, T follicular helper cell; Th1, type 1 T helper; Th2, type 2 T helper; TIL, tumor-infiltrating lymphocyte; Treg, regulatory T cell.

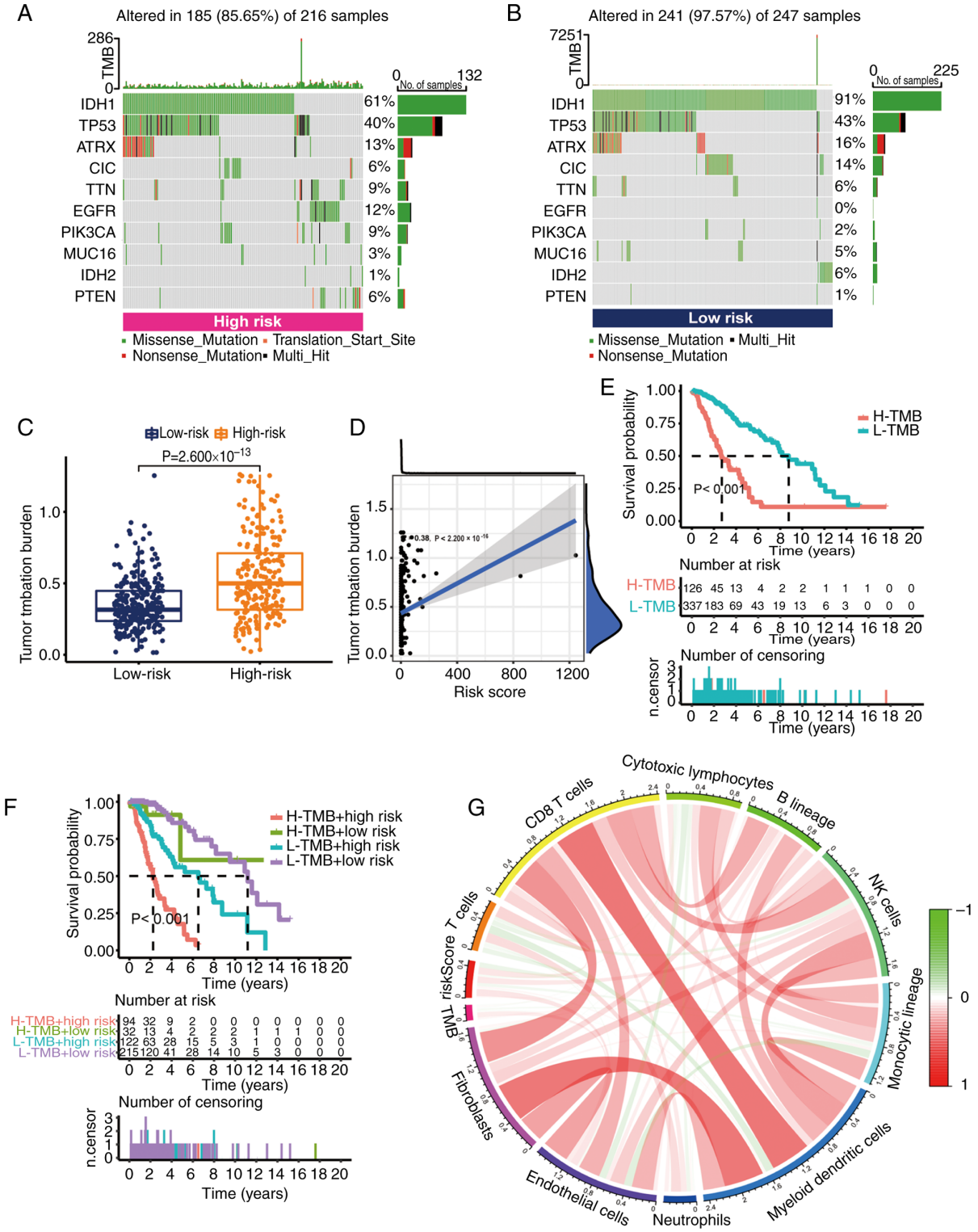

Figure 8. Exploration of TMB targeting risk model. Waterfall plots displaying mutation information of the 10 genes with high mutation frequencies in (A) the high-risk group and (B) the low-risk group. (C) Difference in TMB score between the high- and low-risk groups. (D) Correlation between risk score and TMB. (E) K-M survival curves of the OS of patients in the H-TMB and L-TMB groups. (F) K-M analysis of the OS of the four groups stratified by both TMB and risk score. (G) Correlation between TMB and immune cell subtype. H-, high; K-M, Kaplan-Meier; L-, low; NK, natural killer; OS, overall survival; TMB, tumor mutation burden.

that the TMB score was significantly increased in the high-risk group (Fig. 8C). Additionally, a positive correlation between risk score and TMB was demonstrated by Spearman correlation analysis. According to the median TMB score, grade II-III glioma samples were divided into two groups: High TMB group and low TMB group. According to the results of K-M analysis, the OS of the high TMB group was worse (Fig. 8E). When both risk score and TMB were considered in the K-M analysis, the risk score eliminated the better OS of low TMB. This suggested that the risk score could

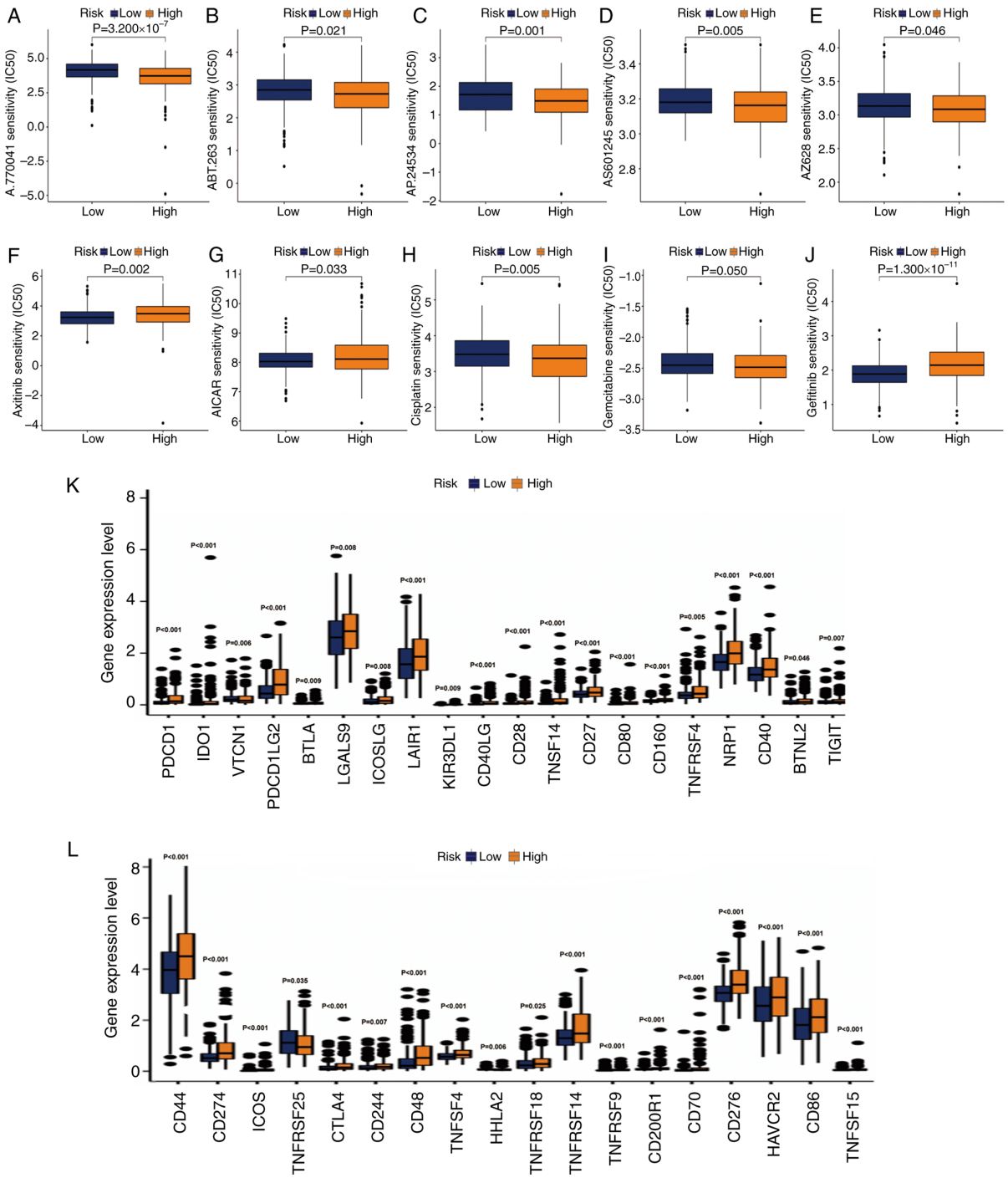

Figure 9. Exploration of potential drugs and assessment of immunotherapy response. (A-G) Analysis of potential drug sensitivity in the two groups. (H-J) Analysis of common chemotherapeutic sensitivity. (K and L) Expression levels of immune checkpoint genes in the two groups. AICAR, 5-aminoimidazole-4-carboxamide ribonucleotide.

predict the prognosis of grade II-III glioma in a superior way than TMB (Fig. 8F). At the same time, the main immune cells associated with TMB were CD8 T cells and natural killer cells (Fig. 8G).

Exploration of potential drugs and assessment of immunotherapy response. Considering the significant difference in prognosis between the two groups of grade II-III glioma samples, some potential drugs for precise treatment were selected. It was hypothesized that the response to drugs may be different between the two groups. The R package 'pRRophetic' was used to screen potential drugs based on the IC_{50} value in the GDSC genomics database. The IC_{50} estimates of A.770041, ABT.263, AP.24534, AS601245 and AZ628 were relatively high in low-risk samples.

This suggested that patients with grade II-III glioma in the high-risk group may benefit from the use of these compounds (Fig. 9A-J). The IC_{50} values of axitinib and 5-aminoimidazole-4-carboxamide ribonucleotide were increased in the high-risk group, indicating that these two drugs may be used

for the treatment of patients with grade II-III glioma in the low-risk group (Fig. 9F and G). The IC_{50} of commonly used antitumor drugs in the two groups was determined. In the low-risk group, the IC_{50} of cisplatin (Fig. 9H) and gemcitabine (Fig. 9I) was higher. The IC_{50} of gefitinib was higher in the high-risk group (Fig. 9J), indicating that the risk score had high accuracy in predicting the sensitivity to antitumor drugs. Finally, it was explored whether the activation of immune checkpoint genes was consistent in the two groups. Consistent with our hypothesis, the activation of immune checkpoint genes in high-risk populations was generally relatively high (Fig. 9K and L).

Functional enrichment analysis. In order to examine the mechanism that leads to significant differences between the two groups in a multi-level analysis, Gene Ontology (GO) and KEGG analyses were performed on 89 DEGs ($|\log_2$ fold change$|>2.0$; $P<0.05$; Table SVI). According to GO analysis (Fig. 10A; Table SVII), DEGs were mainly enriched in tissue-related BPs. In terms of molecular functions, these DEGs were mainly concentrated in 'extracellular matrix structural constituent' and 'glycosaminoglycan binding'. In addition, KEGG analysis showed that the DEGs were concentrated in 'extracellular structure organization' (Fig. 10B and C; Table SVII). Subsequently, through GSEA of KEGG, it was revealed that the pathways enriched in the high-risk (Fig. 10D; Table SVIII) and low-risk (Fig. 10E; Table SVIII) groups were different. Finally, a lncRNA-mRNA interaction network was constructed using Cytoscape software (Fig. 10F). The aforementioned results may provide some ideas regarding the mechanism of glycolysis-related lncRNAs in grade II-III glioma carcinogenesis.

CRNDE is highly expressed in SHG-44 cells and regulates proliferation. Due to the extensive research on CRNDE, CRNDE was chosen for validation (39,40). The high CRNDE expression in grade II-III glioma was verified using cell lines. The experiments revealed high CRNDE expression in SHG-44 cells compared with HA1800 cells (Fig. 11A). In addition, the effects of CRNDE on cell functions were investigated. The function of CRNDE in SHG-44 cells was investigated via knockdown experiments and RT-qPCR confirmed that CRNDE was knocked down in SHG-44 cells (Fig. 11B). The results of the CCK-8 assay indicated that CRNDE could increase cell viability, which was the same as the results of database analysis (Fig. 11C). The colony formation assay also indicated that knockdown of CRNDE significantly inhibited the proliferation of SHG-44 cells (Fig. 11D and E). In addition, the potential regulatory role of CRNDE in glucose metabolism in grade II-III glioma was investigated using the ECAR method. The results demonstrated that knockdown of CRNDE reduced the ECAR and glycolysis (Fig. 11F and G). The experiments further confirmed the results of previous analyses.

Discussion

Grade II-III glioma is rare among adult CNS tumors, but accounts for the highest proportion of childhood CNS neuromalignancies (41,42). Preserving isocitrate dehydrogenase-mutated cell lines has been difficult, limited by the high heterogeneity of low-grade glioma, and thus, there has been little research on this tumor, early clinical diagnosis methods, prognosis prediction and precise treatment. However, with the deepening of research on other tumors, it has been found that lncRNAs are multifunctional tumor regulators. For example, LINC00473 overexpression inhibits microRNA (miR)-502-3p via the competing endogenous RNA mechanism, upregulates the expression of lysine methyltransferase 5A, promotes the expression of cyclin D1 and CDK2, and facilitates cell cycle progression (43,44). In addition, research on the metabolic processes of tumor cells has also gained increasing attention. Among them, glucose metabolism, as a key process of biological energy metabolism, has been widely studied in the regulation of tumor progression (45,46). These frontier hotspots in tumor research were also the starting point of the present study.

The present study used univariate/multivariate Cox regression analysis and LASSO regression analysis to identify seven lncRNAs (CRNDE, AC022034.1, RHOQ-AS1, AL159169.2, AL133215.2, AC007098.1 and LINC02587). Among these lncRNAs, CRNDE has been extensively studied (39,47). In previous studies, CRNDE has been considered to be an important oncogenic lncRNA and Han *et al* (48) pointed out in 2017 that this lncRNA could cross-act with miR-181a-5p and ultimately regulate colon cancer cells through the Wnt signaling pathway proliferation and increase its drug resistance. A similar study by Zhang *et al* (49) also indicated that CRNDE could mediate the resistance of gastric cancer cells to 5-FU/oxaliplatin by altering the apoptosis process of gastric cancer cells by regulating alternative splicing events. Notably, CRNDE is a confirmed oncogenic lncRNA that is upregulated in gliomas and studies have also confirmed that knocking down the expression of this lncRNA can help improve the drug resistance of gliomas (50,51). Although the mechanism of this lncRNA in the process of glycolysis is still unclear, a number of studies have indicated that the process of glycolysis is directly related to the proliferation, migration and apoptosis of tumor cells, which is consistent with the role of CRNDE in other studies and which also confirms the way the lncRNA may function (52,53). The present study verified the levels of CRNDE not only using bioinformatics analysis but also using RT-qPCR. The present study demonstrated that CRNDE could significantly increase SHG-44 cell viability and proliferation. There are fewer studies on AC022034.1 and AC007098.1. Wang *et al* (54,55) used bioinformatics analysis to identify four key lncRNAs involved in the regulation of the TME in colon cancer and pointed out that the lncRNA was also involved in the immune process of this cancer. There are no corresponding research reports for the remaining four lncRNAs, which may be novel directions for future research. To the best of the authors' knowledge, the present study was the first to report that the HR of RHOQ-AS1 suggested that the risk value of RHOQ-AS1 was particularly high and further exploration needs to be continued to improve the related research in the future. A number of studies have shown that the abnormal glycolytic process of cells can cause changes in the composition and biological properties of the TME (56,57). Therefore, a similar exploration was also carried out in the present study. The degree of infiltration of various T cell subtypes increased significantly as the risk increased. A major

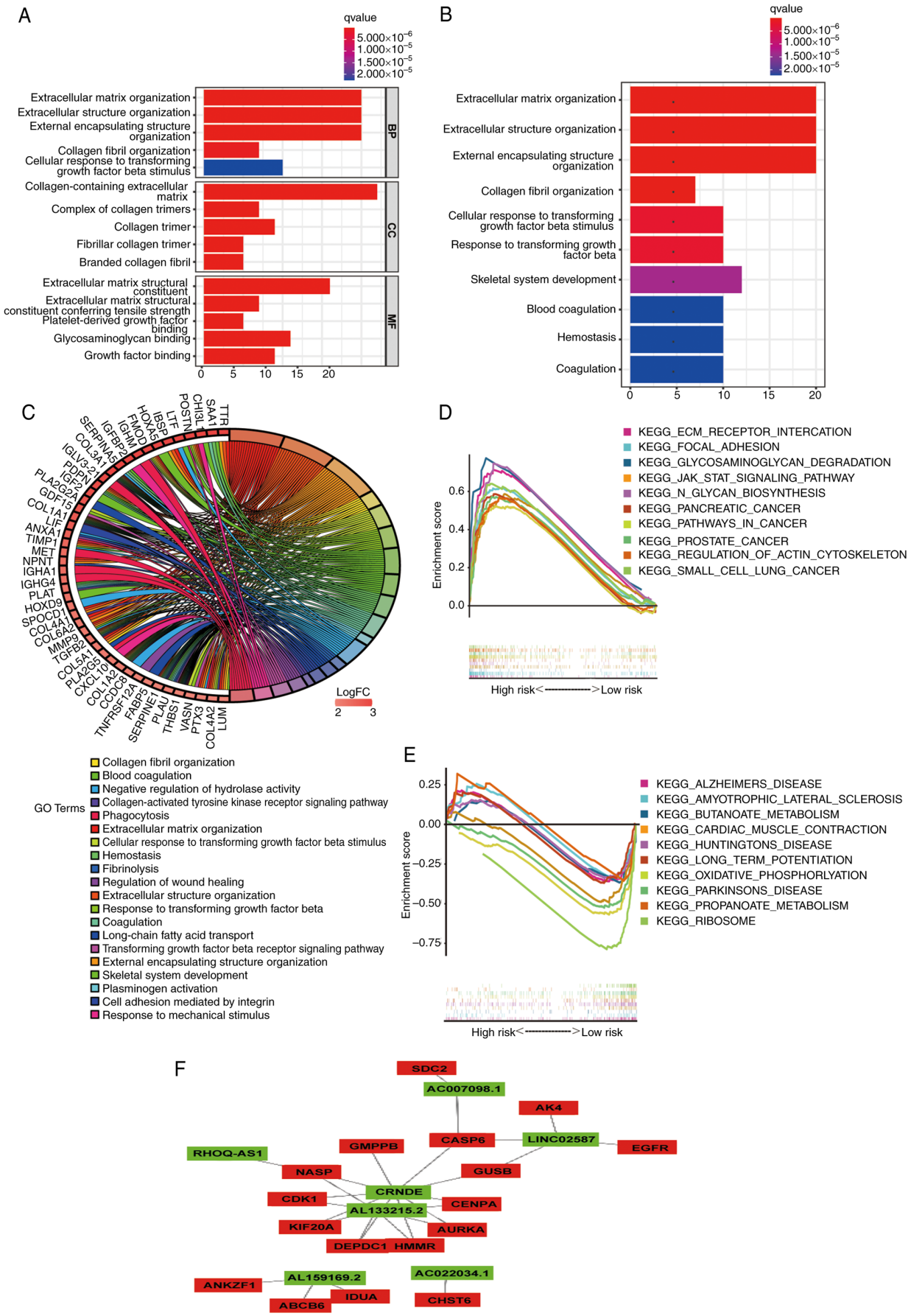

Figure 10. Functional enrichment analyses. (A) GO analysis based on DEGs between high- and low-risk groups. (B and C) KEGG analysis based on DEGs between high- and low-risk groups. (D and E) Gene Set Enrichment Analysis. (F) lncRNA-mRNA co-expression network generated using Cytoscape. Green nodes represent lncRNAs and red nodes represent mRNAs. GO, Gene Ontology; DEG, differentially expressed gene; KEGG, Kyoto Encyclopedia of Genes and Genomes; lncRNA, long non-coding RNA;

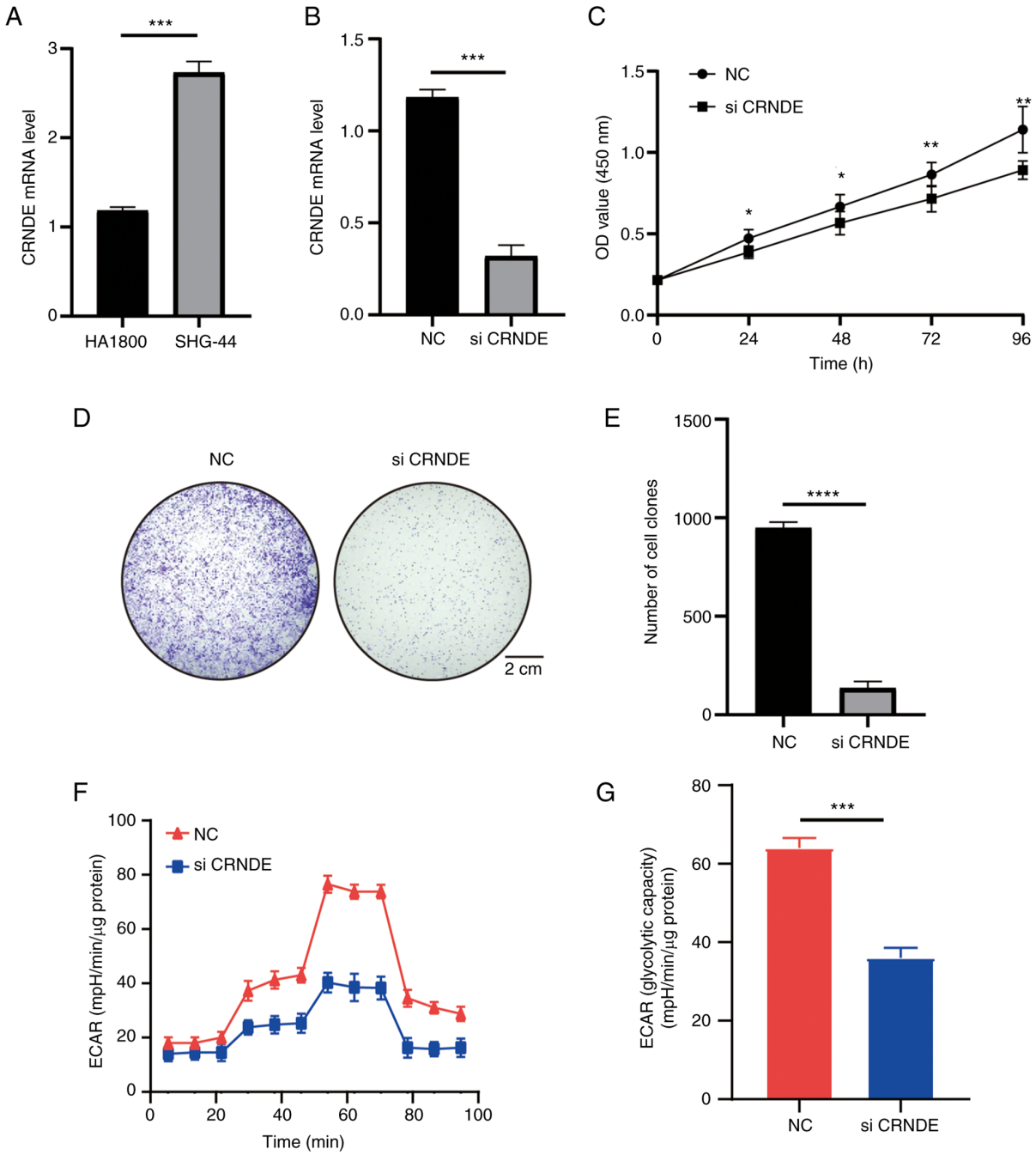

Figure 11. CRNDE and its functional effect on SHG-44 cells. (A) RT-qPCR was used to verify the high CRNDE expression in SHG-44 cells. (B) Knockdown of CRNDE in SHG-44 cells was demonstrated by RT-qPCR. (C) Cell Counting Kit-8 assay of SHG-44 cells after the knockdown of CRNDE. (D and E) Viability was evaluated using colony formation assays in SHG-44 cells. (F and G) ECAR values and calculated glycolytic capacity. Each assay was replicated three times. *P<0.05; **P<0.01; ***P<0.001; ****P<0.0001. RT-qPCR, reverse transcription-quantitative PCR; ECAR, extracellular acidification rate; NC, negative control; OD, optical density; si, small interfering RNA.

study by Peng *et al* (58) in 2016 revealed that glycolysis (the Warburg effect) promoted the maturation and activation of T cells (especially type 1 T helper cells) and in this activation process, IFN-γ (type II-IFN) served a key role, which is consistent with the present results. A comprehensive study by D'Angelo *et al* (59) indicated that ~50% of patients with grade II-III glioma exhibited enhanced T lymphocyte infiltration. A study by Guo *et al* (60) revealed that $CD8^{+}$ T cells activated and released chemokine ccl4 in grade II-III glioma and produced a cascade effect that led to further release of chemokine ccl5 from microglia, which ultimately promoted the progression of grade II-III glioma. Combined with the results of the present analysis, it can be inferred that the higher the degree of infiltration of the T cell population, the more improved the prognosis of the patients. External validation of model effectiveness is an important part of evaluating model generalization ability and practical application potential. The present study attempted to externally validate the model in three CGGA datasets (CGGA301, CGGA325 and CGGA693). Unfortunately, it was not possible to retrieve all the lncRNAs involved in the model in the above three data sets, so external verification could not be performed for at present. This may

be due to the large differences in the detection of lncRNA in different sequencing batches. This suggests that it is necessary to conduct a sufficient depth of lncRNA sequencing for patient samples during the clinical transformation of the model.

Functional enrichment analysis suggested that extracellular matrix-related pathways were significantly altered in patients with grade II-III glioma. The latest study by Tao *et al* (61) indicated that matrix stiffness could increase the malignancy of glioma cells through the activation of the Wnt signaling pathway. The Wnt pathway and glycolysis are closely related in the progression of tumor cells. For example, Jiang *et al* (62) revealed that activating Toll-like receptor 9 could simultaneously inhibit the activation and infiltration of macrophages in HCC brought about by the Wnt pathway and glycolysis. Similarly, Fan *et al* (63) found that autophagy could upregulate glycolysis in HCC cells through the Wnt pathway and deteriorate tumor cell invasion. Although the present study did not directly identify the enrichment of the Wnt pathway, other studies (64,65) have suggested that the Wnt pathway affects tumor progression by regulating glucose metabolism and they may be tightly connected through the extracellular matrix together.

In conclusion, the present study used a large sample of human grade II-III glioma in a database, and screened out seven key lncRNAs related to glycolysis to construct a good model that could accurately predict the prognosis of patients with grade II-III glioma. Multiple aspects of grade II-III glioma were further examined, including the biology and molecular mechanism of drug resistance. In addition, the aforementioned analyses were verified by cell function experiments, aiming to provide novel ideas for the clinical diagnosis of grade II-III glioma.

Acknowledgements

Not applicable.

Funding

No funding was received.

Availability of data and materials

The data generated in the present study may be requested from the corresponding author.

Authors' contributions

TY designed the implementation of the research. RZ and ZC made contributions to the acquisition of data. BZ and XZ participated in the research design and implementation. QH and XY participated in the analysis and interpretation of data. All authors read and approved the final version of the manuscript. RZ and ZC confirm the authenticity of all the raw data.

Ethics approval and consent to participate

Not applicable.

Patient consent for publication

Not applicable.

Competing interests

The authors declare that have no competing interests.

References

1. Ostrom QT, Patil N, Cioffi G, Waite K, Kruchko C and Barnholtz-Sloan JS: CBTRUS Statistical Report: Primary Brain and Other Central Nervous System Tumors Diagnosed in the United States in 2013-2017. Neuro Oncol 22 (12 Suppl 2): iv1-iv96, 2020.
2. Ostrom QT, Bauchet L, Davis FG, Deltour I, Fisher JL, Langer CE, Pekmezci M, Schwartzbaum JA, Turner MC, Walsh KM, *et al*: The epidemiology of glioma in adults: A 'state of the science' review. Neuro Oncol 16: 896-913, 2014.
3. Cancer Genome Atlas Research Network; Brat DJ, Verhaak RG, Aldape KD, Yung WK, Salama SR, Cooper LA, Rheinbay E, Miller CR, Vitucci M, *et al*: Comprehensive, Integrative Genomic Analysis of Diffuse Lower-Grade Gliomas. N Engl J Med 372: 2481-2498, 2015.
4. Okita Y, Narita Y, Miyahara R, Miyakita Y, Ohno M and Shibui S: Health-related quality of life in long-term survivors with Grade II gliomas: The contribution of disease recurrence and Karnofsky Performance Status. Jpn J Clin Oncol 45: 906-913, 2015.
5. Batsios G, Viswanath P, Subramani E, Najac C, Gillespie AM, Santos RD, Molloy AR, Pieper RO and Ronen SM: PI3K/mTOR inhibition of IDH1 mutant glioma leads to reduced 2HG production that is associated with increased survival. Sci Rep 9: 10521, 2019.
6. Zhang C, Yu R, Li Z, Song H, Zang D, Deng M, Fan Y, Liu Y, Zhang Y and Qu X: Comprehensive analysis of genes based on chr1p/19q co-deletion reveals a robust 4-gene prognostic signature for lower grade glioma. Cancer Manag Res 11: 4971-4984, 2019.
7. Ganapathy-Kanniappan S and Geschwind JF: Tumor glycolysis as a target for cancer therapy: Progress and prospects. Mol Cancer 12: 152, 2013.
8. Liberti MV and Locasale JW: The warburg effect: How does it benefit cancer cells? Trends Biochem Sci 41: 211-218, 2016.
9. Locasale JW and Cantley LC: Metabolic flux and the regulation of mammalian cell growth. Cell Metab 14: 443-451, 2011.
10. Ganapathy-Kanniappan S: Molecular intricacies of aerobic glycolysis in cancer: Current insights into the classic metabolic phenotype. Crit Rev Biochem Mol Biol 53: 667-682, 2018.
11. Liu YC, Lin P, Zhao YJ, Wu LY, Wu YQ, Peng JB, He Y and Yang H: Pan-cancer analysis of clinical significance and associated molecular features of glycolysis. Bioengineered 12: 4233-4246, 2021.
12. Yang J, Ren B, Yang G, Wang H, Chen G, You L, Zhang T and Zhao Y: The enhancement of glycolysis regulates pancreatic cancer metastasis. Cell Mol Life Sci 77: 305-321, 2020.
13. Liu Z, Liu Z, Zhou X, Lu Y, Yao Y, Wang W, Lu S, Wang B, Li F and Fu W: A glycolysis-related two-gene risk model that can effectively predict the prognosis of patients with rectal cancer. Hum Genomics 16: 5, 2022.
14. Reuss AM, Groos D, Buchfelder M and Savaskan N: The Acidic Brain-Glycolytic switch in the microenvironment of malignant glioma. Int J Mol Sci 22: 5518, 2021.
15. Alexander RP, Fang G, Rozowsky J, Snyder M and Gerstein MB: Annotating non-coding regions of the genome. Nat Rev Genet 11: 559-571, 2010.
16. Fan C, Tang Y, Wang J, Xiong F, Guo C, Wang Y, Zhang S, Gong Z, Wei F, Yang L, *et al*: Role of long non-coding RNAs in glucose metabolism in cancer. Mol Cancer 16: 130, 2017.
17. Zhao N, Zhang J, Zhao Q, Chen C and Wang H: Mechanisms of long Non-Coding RNAs in biological characteristics and aerobic glycolysis of glioma. Int J Mol Sci 22: 11197, 2021.
18. Zhao L, Ji G, Le X, Wang C, Xu L, Feng M, Zhang Y, Yang H, Xuan Y, Yang Y, *et al*: Long noncoding RNA LINC00092 acts in Cancer-Associated fibroblasts to drive glycolysis and progression of ovarian cancer. Cancer Res 77: 1369-1382, 2017.
19. Sun X, Huang X, Sun X, Chen S, Zhang Z, Yu Y and Zhang P: Oxidative Stress-Related lncRNAs are potential biomarkers for predicting prognosis and immune responses in patients With LUAD. Front Genet 13: 909797, 2022.
20. Chen C, Liu YQ, Qiu SX, Li Y, Yu NJ, Liu K and Zhong LM: Five metastasis-related mRNAs signature predicting the survival of patients with liver hepatocellular carcinoma. BMC Cancer 21: 693, 2021.

21. Zhao J, Wang L and Wei B: Identification and validation of an energy Metabolism-Related lncRNA-mRNA signature for Lower-Grade glioma. Biomed Res Int 2020: 3708231, 2020.
22. Sun X, Song J, Lu C, Sun X, Yue H, Bao H, Wang S and Zhong X: Characterization of cuproptosis-related lncRNA landscape for predicting the prognosis and aiding immunotherapy in lung adenocarcinoma patients. Am J Cancer Res 13: 778-801, 2023.
23. Jerome Friedman TH and RT: Regularization paths for generalized linear models via coordinate descent. J Stat Softw 33: 1-22, 2010.
24. Wu X, Sui Z, Zhang H, Wang Y and Yu Z: Integrated analysis of lncRNA-Mediated ceRNA network in lung adenocarcinoma. Front Oncol 10: 554759, 2020.
25. He Y, Zhang J, Chen Z, Sun K, Wu X, Wu J and Sheng L: A seven-gene prognosis model to predict biochemical recurrence for prostate cancer based on the TCGA database. Front Surg 9: 923473, 2022.
26. Iasonos A, Schrag D, Raj GV and Panageas KS: How to build and interpret a nomogram for cancer prognosis. J Clin Oncol 26: 1364-1370, 2008.
27. Zhuang W, Sun H, Zhang S, Zhou Y, Weng W, Wu B, Ye T, Huang W, Lin Z, Shi L and Shi K: An immunogenomic signature for molecular classification in hepatocellular carcinoma. Mol Ther Nucleic Acids 25: 105-115, 2021.
28. Chakraborty H and Hossain A: R package to estimate intracluster correlation coefficient with confidence interval for binary data. Comput Methods Programs Biomed 155: 85-92, 2018.
29. Mayakonda A, Lin DC, Assenov Y, Plass C and Koeffler HP: Maftools: Efficient and comprehensive analysis of somatic variants in cancer. Genome Res 28: 1747-1756, 2018.
30. Wang Z, Li J, Zhang P, Zhao L, Huang B, Xu Y, Wu G and Xia Q: The Role of ERBB signaling pathway-related genes in kidney renal clear cell carcinoma and establishing a prognostic risk assessment model for patients. Front Genet 13: 862210, 2022.
31. Geeleher P, Cox N and Huang RS: pRRophetic: An R package for prediction of clinical chemotherapeutic response from tumor gene expression levels. PLoS One 9: e107468, 2014.
32. Ritchie ME, Phipson B, Wu D, Hu Y, Law CW, Shi W and Smyth GK: limma powers differential expression analyses for RNA-sequencing and microarray studies. Nucleic Acids Res 43: e47, 2015.
33. Yu G, Wang LG, Han Y and He QY: clusterProfiler: An R package for comparing biological themes among gene clusters. OMICS 16: 284-287, 2012.
34. Brunson JC: Ggalluvial: Layered grammar for alluvial plots. J Open Source Softw 5: 2017, 2020.
35. Li XN, Du ZW and Huang Q: Modulation effects of hexamethylene bisacetamide on growth and differentiation of cultured human malignant glioma cells. J Neurosurg 84: 831-838, 1996.
36. Gulhan PY, Eroz R, Ataoglu O, İnce N, Davran F, Öztürk CE, Gamsızkan Z and Balbay OA: The evaluation of both the expression and serum protein levels of Caspase-3 gene in patients with different degrees of SARS-CoV2 infection. J Med Virol 94: 897-905, 2022.
37. Livak KJ and Schmittgen TD: Analysis of relative gene expression data using real-time quantitative PCR and the 2(-Delta Delta C(T)) method. Methods 25: 402-408, 2001.
38. Feng Q, Qian C and Fan S: A hypoxia-related long non-coding RNAs signature associated with prognosis in lower-grade glioma. Front Oncol 11: 771512, 2021.
39. Lu Y, Sha H, Sun X, Zhang Y, Wu Y, Zhang J, Zhang H, Wu J and Feng J: CRNDE: An oncogenic long non-coding RNA in cancers. Cancer Cell Int 20: 162, 2020.
40. Zhang J, Yin M, Peng G and Zhao Y: CRNDE: An important oncogenic long non-coding RNA in human cancers. Cell Prolif 51: e12440, 2018.
41. Choi S, Yu Y, Grimmer MR, Wahl M, Chang SM and Costello JF: Temozolomide-associated hypermutation in gliomas. Neuro Oncol 20: 1300-1309, 2018.
42. Bale TA and Rosenblum MK: The 2021 WHO classification of tumors of the central nervous system: An update on pediatric low-grade gliomas and glioneuronal tumors. Brain Pathol 32: e13060, 2022.
43. Li J, Qian Y, Zhang C, Wang W, Qiao Y, Song H, Li L, Guo J, Lu D and Deng X: LncRNA LINC00473 is involved in the progression of invasive pituitary adenoma by upregulating KMT5A via ceRNA-mediated miR-502-3p evasion. Cell Death Dis 12: 580, 2021.
44. Zhang X, Gejman R, Mahta A, Zhong Y, Rice KA, Zhou Y, Cheunsuchon P, Louis DN and Klibanski A: Maternally expressed gene 3, an imprinted noncoding RNA gene, is associated with meningioma pathogenesis and progression. Cancer Res 70: 2350-2358, 2010.
45. Vander Heiden MG, Cantley LC and Thompson CB: Understanding the Warburg effect: The metabolic requirements of cell proliferation. Science 324: 1029-1033, 2009.
46. Pavlova NN and Thompson CB: The emerging hallmarks of cancer metabolism. Cell Metab 23: 27-47, 2016.
47. Ma X, Jin W, Zhao C, Wang X and Wang K: CRNDE: A valuable long noncoding RNA for diagnosis and therapy of solid and hematological malignancies. Mol Ther Nucleic Acids 28: 190-201, 2022.
48. Han P, Li JW, Zhang BM, Lv JC, Li YM, Gu XY, Yu ZW, Jia YH, Bai XF, Li L, *et al*: The lncRNA CRNDE promotes colorectal cancer cell proliferation and chemoresistance via miR-181a-5p-mediated regulation of Wnt/β-catenin signaling. Mol Cancer 16: 9, 2017.
49. Zhang F, Wang H, Yu J, Yao X, Yang S, Li W, Xu L and Zhao L: LncRNA CRNDE attenuates chemoresistance in gastric cancer via SRSF6-regulated alternative splicing of PICALM. Mol Cancer 20: 6, 2021.
50. Momtazmanesh S and Rezaei N: Long non-coding RNAs in diagnosis, treatment, prognosis, and progression of glioma: A State-of-the-Art review. Front Oncol 11: 712786, 2021.
51. Zhao Z, Liu M, Long W, Yuan J, Li H, Zhang C, Tang G, Jiang W, Yuan X, Wu M and Liu Q: Knockdown lncRNA CRNDE enhances temozolomide chemosensitivity by regulating autophagy in glioblastoma. Cancer Cell Int 21: 456, 2021.
52. DeBerardinis RJ, Lum JJ, Hatzivassiliou G and Thompson CB: The biology of cancer: Metabolic reprogramming fuels cell growth and proliferation. Cell Metab 7: 11-20, 2008.
53. Deberardinis RJ, Sayed N, Ditsworth D and Thompson CB: Brick by brick: Metabolism and tumor cell growth. Curr Opin Genet Dev 18: 54-61, 2008.
54. Wang Y, Liu J, Ren F, Chu Y and Cui B: Identification and validation of a four-long non-coding RNA signature associated with immune infiltration and prognosis in colon cancer. Front Genet 12: 671128, 2021.
55. Wang G, Liu P, Li J, Jin K, Zheng X and Xie L: Novel prognosis and therapeutic response model of immune-related lncRNA pairs in clear cell renal cell carcinoma. Vaccines (Basel) 10: 1161, 2022.
56. Vitale I, Manic G, Coussens LM, Kroemer G and Galluzzi L: Macrophages and Metabolism in the Tumor Microenvironment. Cell Metab 30: 36-50, 2019.
57. Wang ZH, Peng WB, Zhang P, Yang XP and Zhou Q: Lactate in the tumour microenvironment: From immune modulation to therapy. EBioMedicine 73: 103627, 2021.
58. Peng M, Yin N, Chhangawala S, Xu K, Leslie CS and Li MO: Aerobic glycolysis promotes T helper 1 cell differentiation through an epigenetic mechanism. Science 354: 481-484, 2016.
59. D'Angelo F, Ceccarelli M, Tala, Garofano L, Zhang J, Frattini V, Caruso FP, Lewis G, Alfaro KD, Bauchet L, *et al*: The molecular landscape of glioma in patients with Neurofibromatosis 1. Nat Med 25: 176-187, 2019.
60. Guo X, Pan Y, Xiong M, Sanapala S, Anastasaki C, Cobb O, Dahiya S and Gutmann DH: Midkine activation of $CD8^+$ T cells establishes a neuron-immune-cancer axis responsible for low-grade glioma growth. Nat Commun 11: 2177, 2020.
61. Tao B, Song Y, Wu Y, Peng T, Peng L, Xia K, Xia X, Chen L and Zhong C: Matrix stiffness promotes glioma cell stemness by activating BCL9L/Wnt/β-catenin signaling. Aging (Albany NY) 13: 5284-5296, 2021.
62. Jiang Y, Han Q, Zhao H and Zhang J: Promotion of epithelial-mesenchymal transformation by hepatocellular carcinoma-educated macrophages through Wnt2b/β-catenin/c-Myc signaling and reprogramming glycolysis. J Exp Clin Cancer Res 40: 13, 2021.
63. Fan Q, Yang L, Zhang X, Ma Y, Li Y, Dong L, Zong Z, Hua X, Su D, Li H and Liu J: Autophagy promotes metastasis and glycolysis by upregulating MCT1 expression and Wnt/β-catenin signaling pathway activation in hepatocellular carcinoma cells. J Exp Clin Cancer Res 37: 9, 2018.
64. Zhou M, He J, Li Y, Jiang L, Ran J, Wang C, Ju C, Du D, Xu X, Wang X, *et al*: N^6-methyladenosine modification of REG1α facilitates colorectal cancer progression via β-catenin/MYC/LDHA axis mediated glycolytic reprogramming. Cell Death Dis 14: 557, 2023.
65. Dong S, Liang S, Cheng Z, Zhang X, Luo L, Li L, Zhang W, Li S, Xu Q, Zhong M, *et al*: ROS/PI3K/Akt and Wnt/β-catenin signalings activate HIF-1α-induced metabolic reprogramming to impart 5-fluorouracil resistance in colorectal cancer. J Exp Clin Cancer Res 41: 15, 2022.